



Evaluation of Image Enhancement Techniques for Electrical Capacitance Tomography Applications

Alfred J Mwambela

Department of Electronics and Telecommunications Engineering, University of Dar es Salaam

P.O. Box 33335, Dar es Salaam, Tanzania.

E-mail: nkomo98@yahoo.com

Received 24 Oct 2022, Revised 18 Feb 2023, Accepted 20 Feb 2023 Published Mar 2023

DOI: <https://dx.doi.org/10.4314/tjs.v49i1.11>

Abstract

The fast generation of images in Electrical Capacitance Tomography (ECT) systems is a desirable feature for many industrial applications. Non-iterative reconstruction algorithms which qualify for this requirement generate poor-quality images. The Linear Back Projection (LBP) is the fastest non-iterative reconstruction algorithm. The challenge is to find a technique to improve the quality of images from LBP at a low computational cost. Image enhancement techniques have been investigated for improving the quality of images reconstructed from the LBP algorithm. Simulated and measured static and dynamic flow data were used in the evaluation. The performance results were benchmarked with results from the Projected Land Weber (PLW) one of the accurate iterative reconstruction algorithms. The Gompertz enhancement algorithm was found to have 3.5 times more computation cost than the LBP reconstruction algorithm and the accuracy of the iterative PLW reconstruction algorithm. This is noteworthy since the algorithm does achieve a good balance between accuracy and speed. The fact that the accuracy gained satisfies the reservoir management standards in the multiphase hydrocarbon production sector is significant in this regard.

Keywords: Electrical Capacitance tomography, Multiphase flow imaging, Maximum entropy thresholding, Gompertz distribution, Image enhancement.

Introduction

An ECT system is one of the image-generating systems developed for industrial process control and monitoring (Beck et al. 1997, Hampel et al. 2022). The images show the permittivity distribution of materials inside a vessel reconstructed from capacitance measurement (Warsito et al. 2007). Electrical Capacitance Tomography (ECT) systems have been widely used in industrial processes such as fluidized beds (Wang and Yang 2021), particulate processes (Wang et al. 2014), and trickle beds (Wang et al. 2011).

The quality of the images and the speed of image generation, limit the integration of ECT systems into online monitoring and

control of industrial processes. The function relating permittivity distribution and measured capacitances is a non-linear problem and cannot be expressed analytically because the problem is ill-posed and ill-conditioned (Zhang et al. 2018). The development of appropriate reconstruction algorithms for ECT systems has been thoroughly studied, with particular emphasis placed on the algorithms' accuracy, complexity, speed, usability (application), and robustness (Cui et al. 2016, Zheng and Peng 2020, Deabes and Bouazza 2021).

Linear model-based (Yang et al. 1999, Guo et al. 2020) and nonlinear model-based (Deabes and Amin 2020, Zheng and Peng 2020, Zhang and Zhang 2021) algorithms are

the two main categories of reconstruction algorithm advancements. Superior images are produced using nonlinear model-based reconstruction techniques, albeit at a speed cost (Zhang and Dai 2021). Both iterative and non-iterative reconstruction techniques are used in linear model-based reconstruction techniques. The reconstructed images produced by non-iterative approaches like LBP (Huang et al. 1992) are of poor quality but are generated fast. Image quality is improved by iterative reconstruction methods such as Projected Land Weber (PLW) (Zhang and Zhang 2021), but speed is sacrificed. For industrial applications to integrate ECT systems into real-time and online monitoring and control, reconstruction methods must be accurate and speedy. Only non-iterative linear model-based reconstruction algorithms can satisfy the speed requirements. Increasing image quality at the lowest possible computational cost is the challenge of non-iterative reconstruction approaches.

In image processing and image enhancement methods are widely used to enhance image quality (Qi et al. 2022). Image enhancement algorithms alter images to enhance their readability or informational value to viewers, or to serve as better input for other automated image processing methods. Enhancing LBP reconstructed image quality has been the subject of extensive investigations (Zheng and Peng 2020). The applications of transform domain enhancement methods resulted in the Filtered LBP (FBP) algorithm, which is commonly used in linear imaging systems (Pan et al. 2009, Pelt and Batenburg 2014). The filtering was possible through analytical reconstruction analysis which is not applicable to nonlinear ECT systems (Zeng 2001). An attempt was made to apply the FBP to ECT systems but with more distorted images, relatively (Wahab et al. 2017). Spatial domain enhancement methods have been investigated in ECT systems. Filtering based on image statistical features (Xie et al. 1992), thresholding based on image entropy (Mwambela et al. 1997), thresholding based on image statistical parameters (Xie et al. 2004), edge detection (Puspanathan et al.

2014), data fitting (Nombo et al. 2014), data decomposition (Sun et al. 2015), and deep learning artificial intelligence (Zheng and Peng 2020) have been reported in the literature. The data fitting algorithm based on the Gompertz function has shown promising performance using simulated data (Nombo et al. 2015). Validation of the observed performance using online static and dynamic data became important.

This article provides an enlarged assessment of the efficacy of the enhancement algorithm for the two-component multiphase flow of oil and gas used in the hydrocarbon production sector. The study has employed more data, including single-frame simulated data, single-frame simulated data covering the whole component fraction range, and multi-frame measured data including both static and dynamic flows. In addition to accuracy, other performance metrics have been included, such as computational costs, usability, and robustness of the algorithms. In order to reduce the computation costs, the performance impact of Gompertz optimization parameters has been examined. Benchmarking of the obtained results was done by comparing them with those from an accurate iterative reconstruction algorithm—the Projected Land Weber (PLW) algorithm, and multiphase metering requirements in the hydrocarbon production sector.

The Gompertz enhancement technique has significantly improved the overall performance of the LBP algorithm in providing quality images. The quality of the images in terms of accuracy is comparable to the iterative reconstruction algorithm, under tested conditions. The algorithm's computational cost is 3.5 times higher than those of the plain LBP. This is noteworthy since the PLW is 2160 times higher than plain LBP to get the same accuracy. In terms of speed and necessary accuracy, the algorithm does a decent job of balancing both. The obtained results are consistent for both simulated and measured data over the full component fraction range, hence robust. The robustness of the algorithm is important to achieve consistency and reliability in data

analysis and interpretation. The overall usability of the algorithm meets the requirements of reservoir management in the hydrocarbon industry.

Materials and Methods

Reconstruction algorithms

The problem of nonlinear reconstruction in ECT systems has been extensively discussed by some authors (Yang and Peng 2003, Yang and Peng 2013, Ye et al. 2015, Cui et al. 2016). Therefore, a brief presentation is provided. In the ECT system, the electric field distribution equation inside the circular pipe is given by $\nabla \cdot [\varepsilon(x, y) \nabla \varphi(x, y)] = 0$ where $\varphi(x, y)$ indicates the electric potential at (x, y) , and $\varepsilon(x, y)$ signifies the relative permittivity. The forward problem in ECT can be given by $C = SG + e$, where S , is the sensitivity distribution matrix formed by all the sensitivity maps corresponding to the different electrode pairs in the sensor, C is the normalized capacitances vector, G the permittivity distribution vector representing grey level values in the reconstructed image, and e is the measurement noise, and error vector. The inverse problem can be given by $G = S^{-1}C$. In general, S^{-1} does not exist therefore other methods for the solution must be used (Yang and Peng 2003).

Linear Back Projection (LBP)

Consider S to be a linear mapping from G to C , then S^T can be considered to be related to mapping from C to the G giving an approximation solution given by Eqn. (1) (Xie et al. 1992).

$$G = S^T C \quad (1)$$

Projected Land Weber (PLW)

Find S^{-1} by iteration method based on steepest gradient descent method and the algorithm is expressed in Eqn. (2), where β is a relaxation parameter such that $0.1 < \beta \leq 2$ for faster convergence (Yang et al. 1999).

$$G_{k+1} = P[G_k - \beta S^T(SG_k - C)] \quad (2)$$

$$P = 0 \text{ if } G_k < 0; P = G_k \text{ if } 0 \leq G_k \leq 1; P = 1 \text{ if } G_k > 1$$

Image enhancement algorithms

The following enhancement techniques have been applied to reconstructed images.

Xie image enhancement

The Xie enhancement algorithm is given by Eqn. (3), where $\gamma = \frac{1}{M} \sum_{m=1}^M C_m$ is the average value of the normalized capacitance and $\alpha = \frac{1}{N} \sum_{n=1}^N G_n$ is the average value of the reconstructed permittivity (Xie et al. 1992).

$$\begin{aligned} g &= 0, & \text{if } G_k < (1 - \gamma)\alpha; \\ g &= G_k, & \text{if } (1 - \gamma)\alpha \leq G_k < 1; \\ g &= 1, & \text{if } G_k \geq 1 \end{aligned} \quad (3)$$

Gompertz image enhancement

In image processing, the Gompertz function can be defined by Eqn. (4), such that $\theta_1, \theta_2 > 0$, where θ_1 and θ_2 are parameters to be estimated, g is the new enhanced image and G_k is the reconstructed image (Nombo et al. 2014).

$$g(G_k; \theta_1, \theta_2) = e^{-\theta_1 e^{-\theta_2 G_k}} \quad (4)$$

Thresholding image enhancement

Let n be the total number of grey levels, g number of grey levels such that $g = 0 \dots n$, $p(g)$ the probability function of the tomogram, $P(g) = \sum_{i=0}^g p(i)$ is the cumulative probability of the tomogram. Using entropic thresholding technique (Kapur et al. 1985), the entropy of a tomogram is defined as $H(g) = -\sum_{g=0}^n \frac{p(g)}{P(g)} \log \frac{p(g)}{P(g)}$.

There must exist thresholding grey level s which separate the multiphase flow into oil and gas such that $H(g)$ is a sum of $H_{oil}(s)$ and $H_{gas}(s)$ where,

$$H_O(s) = -\sum_{g=0}^s \frac{p(g)}{P(g)} \log \frac{p(g)}{P(g)} \quad (5)$$

$$H_G(s) = -\sum_{g=s+1}^n \frac{p(g)}{1 - P(g)} \log \frac{p(g)}{1 - P(g)} \quad (6)$$

$$s = \arg \max [H_O(s) + H_G(s)] \quad (7)$$

Simulated and measured capacitance data was used in the analysis. An 8-electrode ECT sensor simulator was used to generate capacitance data for various two-component

flows of oil and gas patterns and regimes given reference patterns (Isaksen and Nordtvedt 1993). Measured capacitance data also referred to as online capacitance data was obtained from an ECT system. Measured static capacitances were obtained from phantoms (Figure 1) that were created based on reference patterns in the simulator. Measured dynamic capacitances were obtained from a multiphase oil and gas test rig (Mwambela and Johansen 2001, Mwambela 2009). In this rig the ECT sensor

is placed at a vertical position, hence only concentric annular flows are generated. An ECT system used was developed at the University of Bergen (Hjertaker 1998). The implemented capacitance transducer is the Ratio Arm Bridge operating at 100 kHz excitation frequency, and capable of generating 100 images per second. The parallel capacitance normalization technique has been used for both simulated and measured capacitances (Baidillah and Takei 2017).

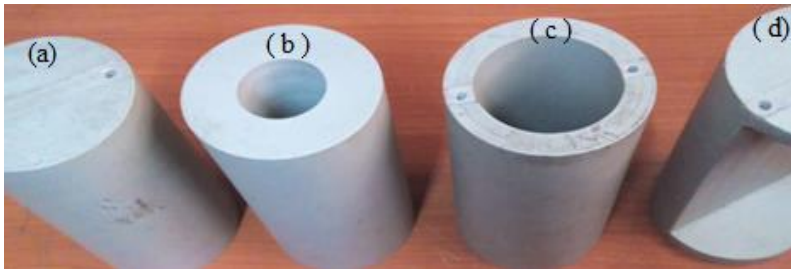


Figure 1: Samples of phantoms made of Perspex material used for measured static capacitances for gas-oil flows. (a) full cross-section, (b) small void fraction annular flow, (c) large void fraction annular flow, and (d) half-full void fraction stratified flow.

To evaluate enhancement techniques, different enhancement algorithms have been implemented based on two reconstruction algorithms, LBP and PLW. Tables 1 and 2 show different enhancement algorithms based

on the LBP reconstruction algorithm. Similar enhancement algorithms based on the PWL reconstruction algorithm can be created by substituting PWL for LBP in Tables 1 and 2.

Table 1: LBP reconstruction algorithms implementing Simple truncation (S), Xie (X) and Gompertz (G) data enhancement techniques followed by the Quantization process (Q)

Algorithms	Description
LBP_SQ	LBP algorithm with simple truncation enhancement
LBP_XQ	LBP algorithm with Xie enhancement
LBP_GQ	LBP algorithm with Gompertz enhancement

Table 2: LBP reconstruction algorithms implementing Simple truncation (S), Xie (X), and Gompertz (G) data enhancement techniques followed by the Thresholding process (T)

Algorithms	Description
LBP_ST	Thresholded LBP algorithm with Simple enhancement
LBP_XT	Thresholded LBP algorithm with Xie enhancement
LBP_GT	Thresholded LBP algorithm with Gompertz enhancement

The quality of the images enhanced by Gompertz algorithm is influenced by the values of optimization parameters θ_1 and θ_2 . To evaluate the influence of Gompertz

optimizing parameters, the Gompertz enhancement algorithm has been implemented in two forms: supervised and unsupervised. In the supervised

implementation, reference data is used to exhaustively obtain the best values of parameters θ_1 and θ_2 . In the unsupervised implementation, optimal parameters are fixed

and used in the measurement of dynamic capacitances or any situation without reference data (Table 3).

Table 3: LBP reconstruction algorithms implementing the Supervise Gompertz (GS) and the Unsupervised Gompertz (GU) parameters estimation techniques

Algorithms	Description
LBP_GS	LBP algorithm with supervised Gompertz enhancement
LBP_GU	LBP algorithm with unsupervised Gompertz enhancement

Data analysis was based on the algorithms' performance under different set conditions. Concentric multiple annular flows, bubble, stratified and annular single frame flows, and annular simulations of all possible component volume fractions.

Performance metrics included accuracy, speed, usability, and robustness of the enhancement algorithms. In this work, accuracy is the closeness of the measured value to a reference value. Spatial similarity distribution error (DE) and gas fraction volumetric estimates gas fraction error (GFE) were used to evaluate accuracy. Spatial similarity analysis compares the enhanced data pixel-by-pixel with the reference set Eqn. (8) where N is the total number of pixels in an image, G_i^{Ref} the i^{th} reference grey level value, and G_i^{Rec} the i^{th} reconstructed grey level value.

$$DE = \frac{1}{N} \sum_{i=1}^N \|G_i^{Ref} - G_i^{Rec}\| \quad (8)$$

The gas volume fraction error (GFE) Eqn. (9) quantifies the absolute difference between the measured gas volume fraction (α_M) and the reference gas volume fraction (α_R),

where $\alpha = \frac{1}{A_{pipe}} \sum_{i=1}^N A_i G_i$, N is the total number of pixel elements, A_i is the area of pixel element i , A_{pipe} is the total area inside the pipe, G_i is the grey level value for pixel i .

$$GFE = \|\alpha_R - \alpha_M\| \quad (9)$$

The speed, the time it takes to process a single frame data set, is used to access the computation cost of the algorithms. Since the LBP is the fastest algorithm, the speed of the enhancement algorithm is evaluated relative to the LBP speed.

Usability in this context is the degree to which an algorithm can be used in multiphase flow measurement. The gas fraction volumetric estimation accuracy performance was benchmarked with metering requirements in the multiphase flow measurement in the hydrocarbon production industry (Table 4) (Thorn et al. 1997).

Robustness in this context is the ability of the algorithm to consistently perform under different set conditions. The superiority of an enhancement algorithm over others should be consistent under set conditions.

Table 4: Typical multiphase meter accuracy requirements in oil production over the full component fraction scale

Oil industry application	Desired volumetric accuracy
Reservoir management	$\sim \pm 10\%$ for all flow phases
Fiscal-Custody transfer	$\pm 2-5\%$ for all flow phases
Fiscal-Taxation/royalty	$\pm 0.25\%$ for oil $\pm 2\%$ for water $\pm 1\%$ for gas

Results

The qualitative visual inspection accuracy evaluation results (Figure 2) show that the LBP-based Gompertz enhancement algorithm improves the quality of the reconstructed images better than the counterpart algorithms. The blurring effect seen in the quantized stages is eliminated by the thresholding enhancement algorithm. However, the effectiveness of enhancement algorithms

depends on the quality of the reconstruction algorithm. The results also highlight the inherent LBP reconstruction algorithm's inability to resolve tiny features like bubble flows (Figure 2, rows 3 & 4). Visual inspection evaluation has the advantage of revealing the nature of distortions introduced in the enhancement process, which are undetectable by quantitative evaluation.

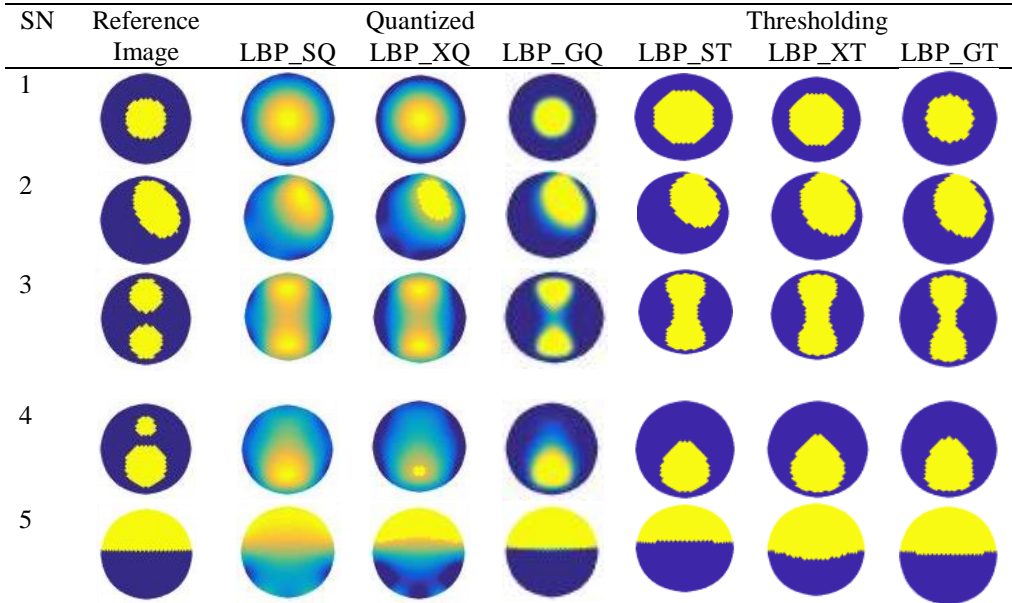


Figure 2: Qualitative visual inspection accuracy performance of enhancement algorithms for simulated sample data of annular, bubble, and stratified gas-oil flows.

To quantify the observed qualitative visual inspection performance, quantitative performance evaluation results are presented (Table 5). Only a quantitative spatial similarity accuracy performance metric (DE

is used for brevity reasons. On average, the results confirm that the Gompertz enhancement algorithm is superior to its counterparts.

Table 5: Quantitative spatial similarity accuracy DE performance of enhancement algorithms for simulated samples of annular, bubble, and stratified gas-oil flows

Reference Image SN	Quantized			Thresholding			
	LBP_SQ	LBP_XQ	LBP_GQ	LBP_ST	LBP_XT	LBP_GT	
1	0.1573	0.3823	0.0891	0.0889	0.3644	0.0889	
2	0.2153	0.2276	0.0679	0.0567	0.1733	0.0678	
3	0.2522	0.3079	0.0868	0.0700	0.2578	0.0867	
4	0.2917	0.3820	0.1335	0.0489	0.3511	0.1333	
5	0.1722	0.1611	0.0101	0.0511	0.1211	0.0100	
Average	0.2178	0.2922	0.0775	0.0631	0.2536	0.0773	

Quantitative performance evaluation was extended to simulated data over the full component fraction range (Figure 3). Overall the Gompertz enhancement algorithm is more effective at enhancing the quality of the reconstructed images than its counterparts over the full component fraction range. Note the enhancement algorithms failures in the extreme ends of the full component fraction range. Large GFE in the lower extreme end

reflects the LBP reconstruction algorithm limitation in resolving small features, particularly at the centre. The results highlight the centre tendency also referred to as the bottom of the valley behaviour for entropic thresholding enhancement algorithm (LBP_ST), where equal components distribution is favoured over the skewed distributions.

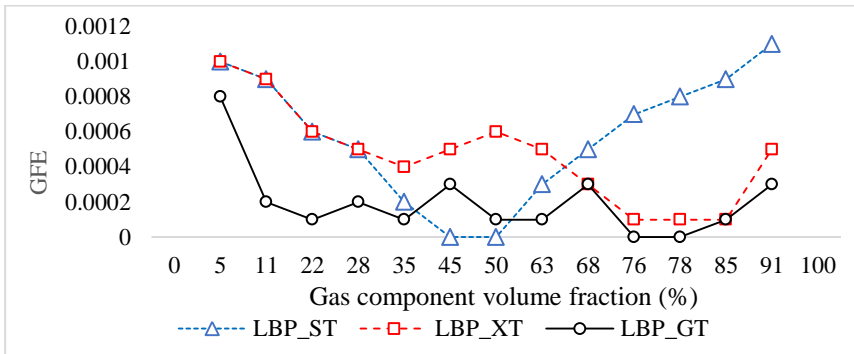


Figure 3: Quantitative gas component fraction volumetric estimation accuracy GFE performance of enhancement algorithms for simulated samples of concentric annular flow data, over full gas volume fraction range.

Similar evaluation was done based on measured static data. The static data contain ECT system noises in contrast to simulated data and has multiple frames of a static flow pattern. Qualitative visual inspection performance (Figure 4) show the Gompertz

enhancement algorithm outperforms its counterparts. On average quantitative evaluation based on DE (Table 6) validates the observed qualitative performance of the enhancement algorithm.

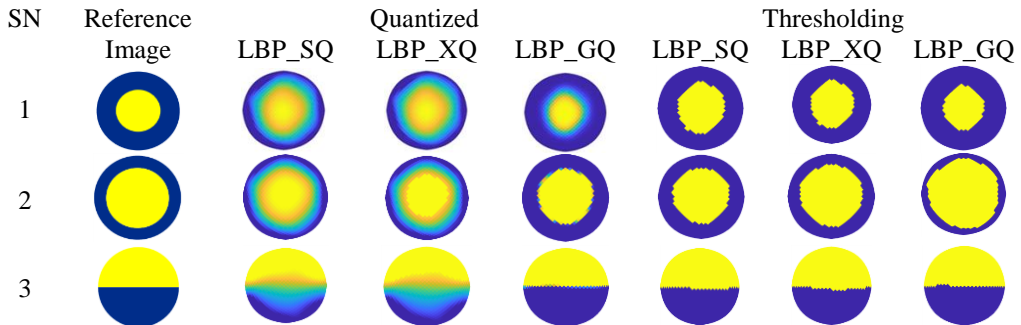


Figure 4: Qualitative visual inspection accuracy performance of enhancement algorithms for measured static (phantom) samples of annular and stratified gas-oil flows.

Table 6: Quantitative spatial similarity accuracy DE performance of the enhancement algorithms for sample static measured phantom data for annular and stratified gas-oil flows

Reference Image SN	Quantized			Thresholding		
	LBP_SQ	LBP_XQ	LBP_GQ	LBP_ST	LBP_XT	LBP_GT
1	0.2263	0.2263	0.0026	0.0956	0.0956	0.0378
2	0.1724	0.1656	0.0353	0.1889	0.1067	0.0667
3	0.1686	0.1680	0.0214	0.0778	0.0878	0.0344
Average	0.1891	0.1866	0.0198	0.1208	0.0967	0.0463

Optimal Gompertz parameters were obtained by varying θ_1 from 100 to 300 at constant θ_2 , and by varying θ_2 at constant θ_1 . In the first case, overall quality increases due

to the larger values of θ_1 (Figure 4). In the latter case, overall quality increases due to the smaller values of θ_2 (Figure 5).

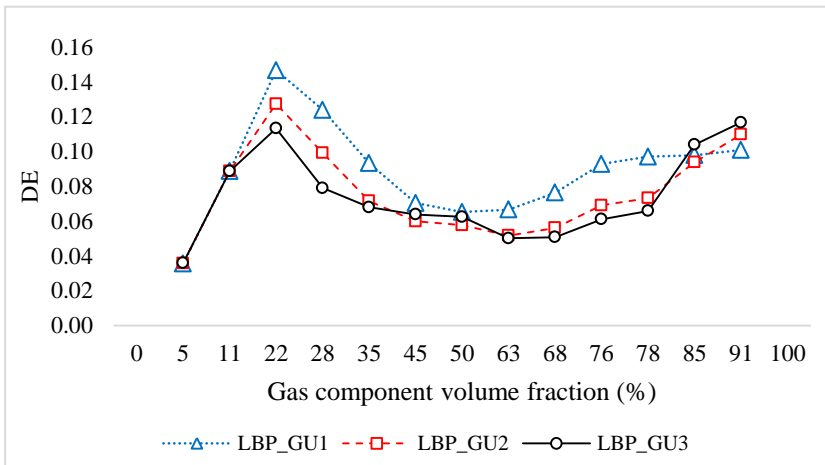


Figure 4: Comparisons of Gompertz unsupervised enhancement algorithms accuracy performance with fixed $\theta_2 = 14$ and varying θ_1 (100, 200 and 300) over the full component fraction range of simulated concentric annular flows.

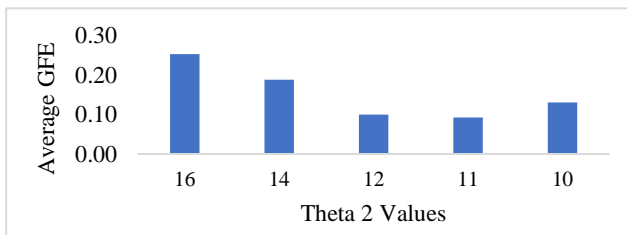


Figure 5: Comparisons of Gompertz unsupervised enhancement algorithms accuracy performance with fixed $\theta_1 = 300$ and varying θ_2 over the full component fraction range of simulated concentric annular flows.

Fixed θ_1 and θ_2 values were utilised to evaluate the enhancement algorithm for measured dynamic capacitance data. Results show that on average Gompertz enhancement algorithm outperforms its counterparts (Figure 6). However, the GFE values are large relative to simulated data. The

measured dynamic data contains both ECT system and test facility noises. Generating a constant flow pattern from the test rig was not practical; hence other undesirable non-concentric annular flow patterns were also present during data acquisition.

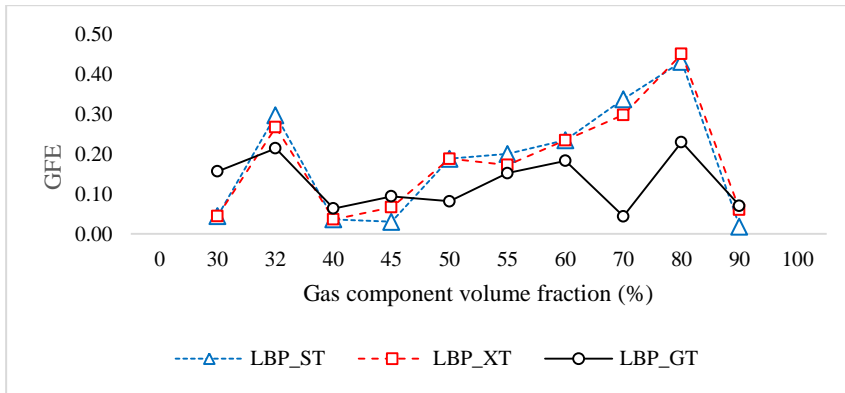


Figure 6: Quantitative gas component volumetric estimation accuracy (GFE) performance of enhancement algorithms for thresholded measured dynamic concentric annular flows data over the full component fraction range.

Figure 7 displays the usability evaluation findings of the Gompertz enhancement algorithm in relation to multiphase flows used in the hydrocarbon production industry. The algorithm's gas component volumetric estimate accuracy (GFE) performance satisfies the taxation condition, which is the strictest of the three requirements (Table 4).

However, the algorithm satisfies the custody transfer condition when considering spatial similarity accuracy (DE) performance. The two performance metrics are different in that GFE is unconcerned with spatial dissimilarity, whereas DE finds it unacceptable.

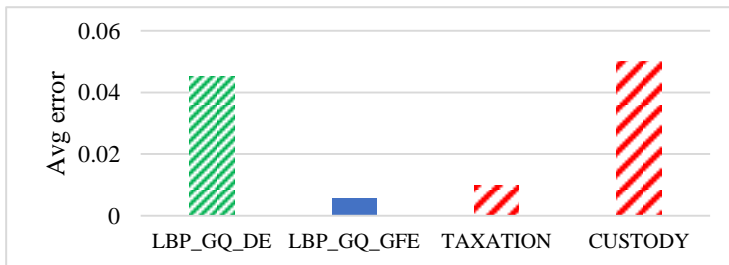


Figure 7: Quantitative accuracy performance using DE and GFE metrics of enhancement algorithms for simulated concentric annular flows over the full component fraction range.

The computational cost evaluation of the enhancement algorithms is shown in Table 7. Static optimal Gompertz parameters have been used. The relative speed of the Gompertz enhancement algorithm is 3.5

times that of the fastest LBP reconstruction, which is reasonable at the accuracy of iterative reconstruction algorithms such as PLW. This is significant as the fine balance between speed and accuracy is established.

Table 7: Comparisons of the speed of enhancement algorithms per single frame

Algorithm	Time(s)	Relative time
LBP_SQ	0.0020	0.00
LBP_XQ	0.0039	0.95
LBP_GQ	0.0090	3.50
PLW_SQ	4.3225	2160

PWL-based enhancement algorithms are used to benchmark the performance of LBP-based enhancement algorithms. Figure 8 displays the findings of the visual inspection examination. There is a relatively less blurring effect in PLW-generated images. However, the PLW-based enhancement algorithms introduce artefacts in images. Artefacts are undesirable pixel elements

introduced in areas of the images where they were originally not present. This problem remains the same for all recommended convergence factors (Li and Yang 2008). The findings also demonstrate the strength of iterative algorithms in resolving small features relative to non-iterative algorithms (Figure 8, row 2).

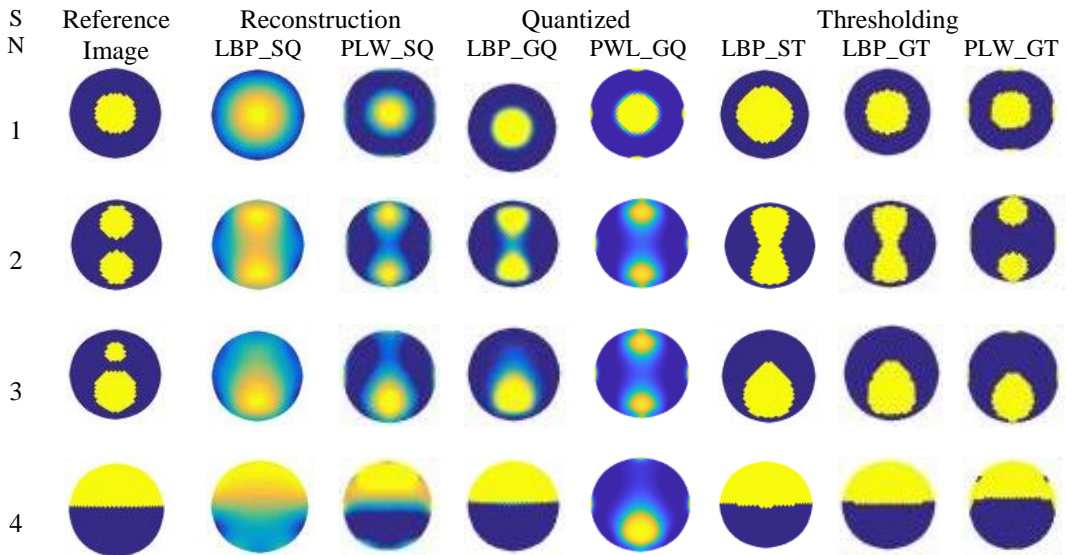


Figure 8: Qualitative visual inspection accuracy performance comparing the performance of the LBP-based and PLW-based enhancement algorithms using simulated sample data of annular, bubble, and stratified gas-oil flows.

Figure 9 shows benchmarking results of simulated data over the full component fraction range using both DE and GFE accuracy performance metrics with standard requirements in multiphase flow in the hydrocarbon industry. The LBP-based Gompertz enhancement algorithm is better

than the PLW-based counterpart. Both enhancement algorithms meet the taxation condition over the full component fraction range using the GFE performance metric. However, they differ when using the DE performance metric.

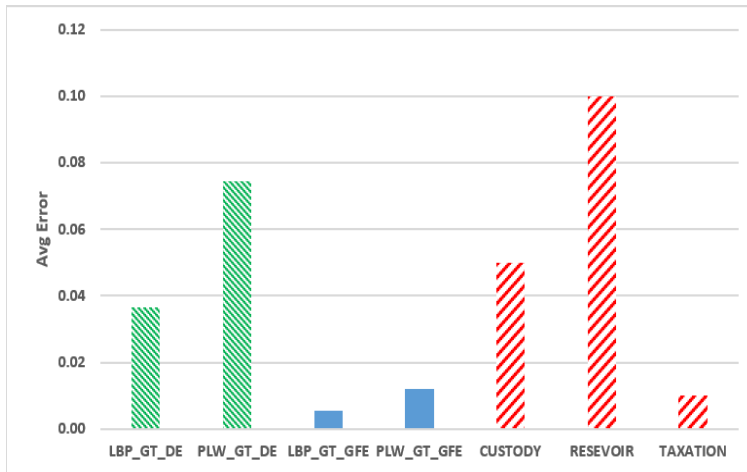


Figure 9: Quantitative comparisons between LBP-based and PLW-based enhancement algorithms using averages of spatial similarity (DE) and gas component volumetric estimation (GFE) accuracy performances for simulated concentric annular flows over the full component fraction range.

The benchmarking analysis was extended to measured dynamic capacitance data (Figure 10). The LBP-based Gompertz enhancement algorithm is still better than its

counterparts. However, none of the two algorithms meet the requirements in multiphase flows used in the hydrocarbon production industry.

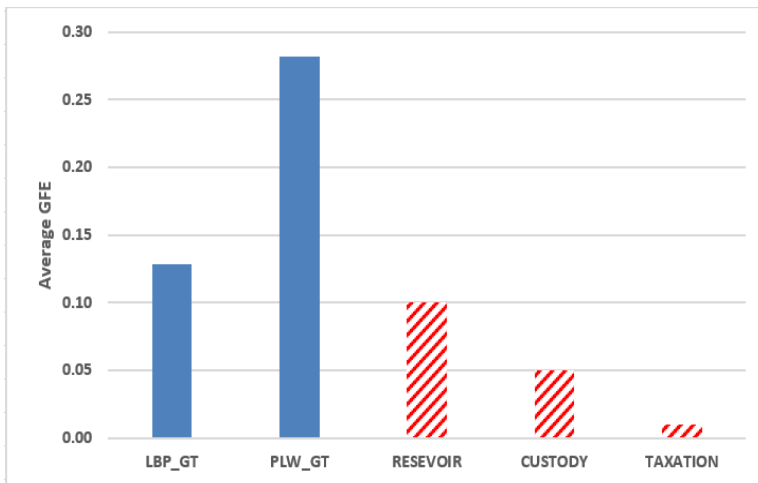


Figure 10: Quantitative comparisons between LBP-based and PLW-based enhancement algorithms using gas component volumetric estimation (GFE) accuracy performance for measured dynamic concentric annular flows over the full component fraction range.

Discussion

This study's major goal was to assess how well the LBP-based enhancement algorithms performed in two-component multiphase flow applications for gas and oil. Improving the image quality at a reasonable computation

cost was a desirable aspect of the assessment. Different data sets simulated and measured static and dynamic data were used in the assessment. Annular, stratified, and bubble flow regimes over the full component fraction range have been used. The evaluation

criteria have been accuracy, speed, usability, and robustness. The outcomes have been benchmarked with the known accurate but computationally intensive iterative PLW-based enhancement algorithm.

Outcomes from the qualitative visual inspection method (Figures 2, 4, and 8), revealed the nature of distortions introduced in the enhancement process. The blurring of sharp transitions and artefacts are some of the distortions observed (Figure 8). The success of enhancement algorithms depends on the reconstruction algorithm used, in this case, LBP or PLW. The LBP-based enhancement algorithms are poor in resolving small features relative to the PLW-based enhancement algorithm (Figure 2 rows 3). However, both have failed to resolve the smallest features (Figure 2 rows 4). It was unexpected that the PLW-based enhancement algorithms would introduce artefacts in the images, which would become more obvious when the images were thresholded.

The quantitative accuracy performance metrics DE and GFE have been employed. The DE metric has a drawback in that it can only be applied to measured static or simulated data, as it needs reference data to function (Figure 4 and Tables 5 and 6). The fact that DE by design recognises spatial dissimilarity while GFE does not means the artefacts created by PLW-based algorithms will be recognised by DE but not by GFE. DE values will therefore always be greater than GFE values (Figures 7 and 9). The GFE metric has been deployed in assessing the full component fraction range for simulated and measured dynamic data (Figures 3 and 6, respectively) and benchmarking LBP-based over PLW-based enhance algorithms (Figure 10). It is a noteworthy accomplishment that the LBP-based Gompertz enhancement algorithm outperforms its competitors in terms of overall accuracy because the results are on par with those of PLW iterative reconstruction techniques. Note that in this work the LBP-based Gompertz was more accurate than PLW-based Gompertz enhancement algorithms.

Despite its shortcomings, the LBP reconstruction algorithm is still used by

researchers in part because of its speed. This is currently the most efficient reconstruction algorithm that is suitable for industrial applications. Its lack of accuracy is its fundamental issue; hence one of the research concerns has been how to make it more accurate. Researchers have placed a high priority on developing an algorithm that balances speed and accuracy well. Significant in this regard is the obtained speed of the Gompertz enhancement method, which is 3.5 times the speed of LBP (Table 7) at the accuracy of the iterative reconstruction algorithm.

The LBP-based Gompertz enhancement algorithm satisfies the taxation conditions when GFE is used and the custody transfer conditions when DE is employed, according to a usability test utilising simulated data over complete component fraction data (Figures 7 and 9). The performance essentially satisfies the custody transfer criteria. However, on using online dynamic data the performance closely meets the reservoir management conditions (Figure 10) as previously explained. This is an area that needs further investigation.

The analysis of the enhancement algorithms in this study has been done using a variety of test settings. In every situation, the Gompertz improvement algorithm has consistently outperformed its competitors. In this aspect, the algorithm is regarded as being robust or resilient.

Conclusion

In this article, an LBP-based enhancement algorithm for image quality improvement from ECT systems applicable to two-component multi-phases has been presented. The algorithm has accuracy close to those obtained from iterative reconstruction such as PLW and at 3.5 times the speed of the LBP algorithm. This performance strikes a good balance between the required accuracy and speed of reconstruction for multiphase flows in the oil and gas industry. The preliminary observed performance suggests that the measurement system not only to be useful for reservoir management but also for custody transfer applications in the hydrocarbons

productions industry. More investigations are recommended to assess the dynamic online data taking advantages of advances in ECT system technologies.

Acknowledgement

The author wishes to acknowledge assistance from Josiah Nombo, Shamte Kawambwa and the anonymous reviewers for their useful inputs to this work.

References

- Baidillah MR and Takei M 2017 Exponential model normalization for electrical capacitance tomography with external electrodes under gap permittivity conditions. *Meas. Sci. Technol.* 28(6): 064002.
- Beck MS, Byars M, Dyakowski T, Waterfall R, He R, Wang SJ and Yang WQ 1997 Principles and industrial applications of electrical capacitance tomography. *Meas. Control* 30(7): 197–200.
- Cui Z, Wang Q, Xue Q, Fan W, Zanga L, Cao Z, Sun B, Wang H and Yang W 2016 A review on image reconstruction algorithms for capacitance/resistance tomography. *Sensor Rev.* 36(14).
- Deabes W and Amin HH 2020 Image reconstruction algorithm based on PSO-tuned fuzzy inference system for electrical capacitance tomography. *IEEE Access* 8: 191875–191887.
- Deabes W and Bouazza KE 2021 Efficient image reconstruction algorithm for ECT system using local ensemble transform Kalman filter. *IEEE Access* 9: 12779–12790.
- Guo H, Liu S, Cheng H, Sun S, Ding J and Guo H 2020 Iterative computational imaging method for flow pattern reconstruction based on electrical capacitance tomography. *Chem. Eng. Sci.* 214: 115432.
- Hampel U, About L, Banasiak R, Schleicher E, Soleimani M, Wondrak T, Vauhkonen M, Lähivaara T, Tan C, Hoyle B and Penn A 2022 A review on fast tomographic imaging techniques and their potential application in industrial process control. *Sensors* 22(6): 2309.
- Hjertaker BT 1998 Static characterization of a dual sensor flow imaging system. *Flow Meas. Instrum.* 9(3): 183–191.
- Huang SM, Xie CG, Beck MS, Thorn R and Snowden D 1992 Design of sensor electronics for electrical capacitance tomography. *IEE Proceedings G (Circuits, Devices and Systems)*. IET Digital Library. Retrieved from <http://digital-library.theiet.org/content/journals/10.1049/ip-g-2.1992.0014>
- Isaksen O and Nordtvedt JE 1993 A new reconstruction algorithm for process tomography. *Meas. Sci. Technol.* 4(12): 1464–1475.
- Kapur JN, Sahoo PK, and Wong AKCKC 1985 A new method for gray-level picture thresholding using the entropy of the histogram. *Computer Vision, Graphics, and Image Processing* 29(3): 273–285.
- Mwambela A 2009 The influence of quantization process on the performance of global entropic thresholding algorithms using electrical capacitance tomography data. *Tanz. J. Sci.* 31(2): 63–76.
- Mwambela AJ and Johansen G 2001 Multiphase flow component volume fraction measurement: experimental evaluation of entropic thresholding methods using an electrical capacitance tomography system. *Meas. Sci. Technol.* 12(8): 1092–1101.
- Mwambela AJ, Isaksen, and Johansen GA 1997 The use of entropic thresholding methods in reconstruction of capacitance tomography data. *Chem. Eng. Sci.* 52(13): 2149–2159.
- Nombo J, Mwambela A and Kisangiri M 2014 A grey level fitting mechanism based on Gompertz function for two phase flow imaging using electrical capacitance tomography measurement. *Int. J. Comput. Appl.* 101(8): 7–12.
- Nombo J, Mwambela A, and Kisangiri M 2015 Performance Analysis of Grey Level Fitting Mechanism based Gompertz Function for Image Reconstruction Algorithms in Electrical Capacitance Tomography Measurement System. *Int. J. Comput. Appl.* 109(15): 8887.

- Pan X, Sidky EY and Vannier M 2009 Why do commercial CT scanners still employ traditional, filtered back-projection for image reconstruction? *Inverse Problems* 25(12): 123009.
- Pelt M and Batenburg KJ 2014 Improving filtered backprojection reconstructions from limited data by filter optimization. *IEEE Trans. Image Process.* '14. 23(11): 1–13.
- Qi Y, Yang Z, Sun W, Lou M, Lian J, Zhao W, Deng X and Ma Y 2022 A Comprehensive Overview of Image Enhancement Techniques. *Arch. Comput. Methods Eng.* 29(1): 583–607.
- Thorn R, Johansen GA and Hammer EA 1997 Recent developments in three-phase flow measurement. *Meas. Sci. Technol.* 8(7): 691.
- Wahab YA, Rahim RA, Rahiman MHF, Aw SR, Yunus FRM, Pusppanathan J, Ayob NMN, Ling LP, Rahim HA, Ahmad IL, Jonet A, Seng CK and Sek TK 2017 Inverse problem: Comparison between linear back-projection algorithm and filtered back-projection algorithm in soft-field tomography. *Int. J. Integr. Eng.* 9(4): 32–36.
- Wang A, Marshdeh Q, Motil BJ and Fan LS 2014 Electrical capacitance volume tomography for imaging of pulsating flows in a trickle bed. *Chem. Eng. Sci.* 119: 77–87.
- Wang H, Wang X, Lu Q, Sun Y and Yang W 2011 Imaging gas-solids distribution in cyclone inlet of circulating fluidised bed with rectangular ECT sensor. In *2011 IEEE International Conference on Imaging Systems and Techniques, IST 2011-Proceedings*.
- Wang H and Yang W 2021 Application of electrical capacitance tomography in pharmaceutical fluidised beds—A review. *Chem. Eng. Sci.* 231: 116236.
- Warsito W, Marshdeh Q and Fan LS 2007 Electrical capacitance volume tomography. *IEEE Sensors J.* Xie CG, Huang SM, Beck MS, Hoyle BS, Thorn R, Lenn C and Snowden D 1992 Electrical capacitance tomography for flow imaging: system model for development of image reconstruction algorithms and design of primary sensors. *IEE Proceedings G (Circuits, Devices and Systems)*. 139(1): 89–98.
- Yang W and Peng L 2003 Image reconstruction algorithms for electrical capacitance tomography. *Meas. Sci. Technol.* 14(1): R1.
- Yang WQ, Spink DM, York TA and McCann H 1999 An image-reconstruction algorithm based on Landweber's iteration method for electrical-capacitance tomography. *Meas. Sci. Technol.* 10(11): 1065–1069.
- Yang Y and Peng L 2013 Data pattern with ECT sensor and its impact on image reconstruction. *IEEE Sensors J.* 13(5): 1582–1593.
- Ye J, Wang H and Yang W 2015 Image reconstruction for electrical capacitance tomography based on sparse representation. *IEEE Trans. Instrum. Meas.* 64(1): 89–102.
- Zhang L and Dai L 2021 Image reconstruction of electrical capacitance tomography based on an efficient sparse Bayesian learning algorithm. *IEEE Sensors J.* 21(18): 1558–1748.
- Zhang L, Zhai Y, Wang X and Tian P 2018 Reconstruction method of electrical capacitance tomography based on wavelet fusion. *Meas.: J. Int. Meas. Confed.* 126: 223–230.
- Zhang L and Zhang M 2021 Image reconstruction of electrical capacitance tomography based on optimal simulated annealing algorithm using orthogonal test method. *Flow Meas. Instrum.* 80: 101996.
- Zheng J and Peng L 2020 A deep learning compensated back projection for image reconstruction of electrical capacitance tomography. *IEEE Sensors J.* 20(9): 4879–4890.